Science Bulletin 64 (2019) 918–925

Contents lists available at ScienceDirect

Science Bulletin

journal homepage: www.elsevier.com/locate/scib

Article

Enhanced photocatalytic N_2 fixation by promoting N_2 adsorption with a co-catalyst

Xiang Gao [a,b], Li An [c], Dan Qu [c,*], Wenshuai Jiang [c], Yanxiao Chai [c], Shaorui Sun [c], Xingyuan Liu [a], Zaicheng Sun [c]

[a] *State Key Laboratory of Luminescence and Applications, Changchun Institute of Optics, Fine Mechanics and Physics, Chinese Academy of Sciences, Changchun 130033, China*
[b] *University of Chinese Academy of Sciences, Beijing 100190, China*
[c] *Center of Excellence for Environmental Safety and Biological Effects, Beijing Key Laboratory of Green Catalysis and Separation Department of Chemistry and Chemical Engineering, School of Environmental and Energy, Beijing University of Technology, Beijing 100124, China*

ARTICLE INFO

Article history:
Received 13 April 2019
Received in revised form 29 April 2019
Accepted 6 May 2019
Available online 16 May 2019

Keywords:
N_2 fixation
Photocatalyst
Co-catalyst
N_2 adsorption
NiS

ABSTRACT

Photocatalytic N_2 fixation involves a nitrogen reduction reaction on the surface of the photocatalyst to convert N_2 into ammonia. Currently, the adsorption of N_2 is the limiting step for the N_2 reduction reaction on the surface of the catalyst. Based on the concept of photocatalytic water splitting, the photocatalytic efficiency can be greatly enhanced by introducing a co-catalyst. In this report, we proposed a new strategy, namely, the loading of a NiS co-catalyst on CdS nanorods for photocatalytic N_2 fixation. Theoretical calculation results indicated that N_2 was effectively adsorbed onto the NiS/CdS surface. Temperature programmed desorption studies confirmed that the N_2 molecules preferred to adsorb onto the NiS/CdS surface. Linear sweep voltammetry results revealed that the overpotential of the N_2 reduction reaction was reduced by loading NiS. Furthermore, transient photocurrent and electrochemical impedance spectroscopy indicated that the charge separation was enhanced by introducing NiS. Photocatalytic N_2 fixation was carried out in the presence of the catalyst dispersed in water without any sacrificial agent. As a result, 1.0 wt% NiS/CdS achieved an ammonia production rate of 2.8 and 1.7 mg L^{-1} for the first hour under full spectrum and visible light ($\lambda > 420$ nm), respectively. The catalyst demonstrated apparent quantum efficiencies of 0.76%, 0.39% and 0.09% at 420, 475 and 520 nm, respectively. This study provides a new method to promote the photocatalytic efficiency of N_2 fixation.

1. Introduction

Ammonia (NH_3) is an essential chemical for the biological synthesis of fertilizer. The Haber-Bosch process, as a typical industrial NH_3 synthesis, is carried out at high temperatures (>300 °C) and pressures (>10 MPa) [1], which is an enormous energy- and money- consuming process of N_2 fixation. In nature, nodule bacteria are very good at biological nitrogen fixation at ambient conditions, although the reduction of N_2 to NH_3 is thermodynamically favored because its free energy is negative at ambient temperature and pressure. However, this does not commonly occur because N_2 is stable and inert due to the strong triple bond and low polarizability [2]. Photocatalytic N_2 fixation was reported with the use of wide bandgap TiO_2 about half a century ago. However, progress in the area has been slow [3,4]. The mechanism of N_2 fixation is as follows [5–8]: N_2 absorbs onto the surface of the semiconductor. In the presence of light shining on the semiconductor, the photogenerated electron is transferred to the N_2 molecules. The sturdy triple bonds are weakened so that N_2 can be reduced, with the participation of water molecules. Unfortunately, both the degree of N_2 fixation and the conversion efficiency are quite low due to the inefficient electron transfer from the photocatalyst to N_2 molecules [9]. Thus, the critical issue is how to effectively combine the N_2 molecules with the photocatalyst to promote photogenerated electron transfer to the N_2 molecules and to weaken the triple bonds. Recently, Li et al. [10,11] demonstrated that BiOBr nanosheets with oxygen vacancies can be employed for N_2 fixation. Oxygen vacancies play a critical role in photocatalytic N_2 fixation by serving as an active site to promote the absorbance of N_2 molecules onto the BiOBr surface. On the other hand, oxygen vacancies can also induce a defect band, which is slightly lower than that of the CB of the catalyst. The photogenerated electron easily relaxes from the conduction band to the defect band. Thus, oxygen vacancies

---

* Corresponding author.
E-mail address: danqu@bjut.edu.cn (D. Qu).

https://doi.org/10.1016/j.scib.2019.05.009

bridge the transfer route between the catalyst and the N_2 molecules for the excited electron. Following this idea, a few photocatalysts have been developed for photocatalytic N_2 fixation such as BiOX [12–14], TiO_2 [15,16], WO_x [8,17], g-C_3N_4 [18], LDH [19], and noble metals and alloys [20–22].

Recently, enormous progress has been made at promoting light absorption and charge separation [23–27]. In heterogeneous photocatalytic water splitting, co-catalysts (e.g., Pt nanoparticles) are often employed to promote the adsorption of the proton, enhance the charge separation and lower the overpotential of the surface reaction [28–31]. To increase the efficiency of photocatalytic N_2 fixation, N_2 has to be chemisorbed onto the surface of the catalyst, N_2 has to have a relatively low reduction potential on the catalyst surface and the process has to involve a highly efficient charge separation process. Based on the above analysis, we proposed a new strategy to construct a composite photocatalyst by introducing a co-catalyst to promote N_2 adsorption on the catalyst surface. In the photocatalytic water splitting system, there exists the co-catalyst, such as Pt nanoparticles, which works as a bridge between the catalyst and water molecules. Based on the concept of photocatalytic water splitting, we constructed CdS nanorods loaded with NiS nanosheets as the photocatalyst and co-catalyst composite catalyst. CdS was demonstrated as a visible light photocatalyst in a broad light adsorption range in the visible light region. The theoretical calculation and the results of thermal program desorption (TPD) of N_2 revealed that N_2 absorbs on the (2 1 1) lattice plane of the NiS nanostructure. Linear sweep voltammetry experiments illustrated that the overpotential of the N_2 reduction reaction was lower on NiS/CdS than that on CdS. Furthermore, the photocurrent and electrochemical impedance spectroscopy results indicated that NiS/CdS composites had a higher charge transfer efficiency. The NiS/CdS composite catalyst was further employed for photocatalytic N_2 fixation. The ammonia production rate in the presence of 1.0 wt% NiS/CdS was 2.8 and 1.7 mg L^{-1} h^{-1} for the first hour under full spectrum light and visible light ($\lambda > 420$ nm), respectively, which was much higher than the corresponding N_2 fixation amount of CdS. The apparent quantum efficiency (AQE) of NiS/CdS reached 0.76%, 0.39% and 0.09% at 420, 475 and 520 nm, respectively. ^{15}N labeling experiments showed that the nitrogen source of NH_3 was from N_2 molecules.

2. Materials and methods

All chemicals were of analytical grade and used without further purification. Cadmium acetate dihydrate, sodium nitroprusside and nickel acetate tetrahydrate were purchased from Macklin Co., Ltd. Ethane diamine, hydrazine hydrate, phenol and Nessler's reagent were of AR grade and purchased from J&K Chemicals Co., Ltd. Dimethyl sulfoxide, thiourea and sodium citrate were purchased from Sinopharm Chemical Reagent Co., Ltd. Standard ammonia solution (1,000 mg L^{-1} ammonia in water) was purchased from Sigma-Aldrich Co., Ltd. $^{15}N_2$ gas was purchased from Aladdin Co., Ltd.

2.1. Preparation of CdS nanorods

Approximately 1 mmol of $Cd(Ac)_2{\cdot}2H_2O$ and 2 mmol of thiourea were dissolved in 30 mL of hydrazine hydrate under ultrasonication for 30 min. The solution was transferred into a 100-mL Teflon-lined stainless steel autoclave, heated to 180 °C and maintained at this temperature for 24 h. Thereafter, CdS nanorods were obtained by centrifugation and washed with ethanol and DI water several times. Finally, they were dried at 60 °C in an oven for 12 h.

2.2. Preparation of NiS/CdS nanorods

Approximately 0.034 mmol of $Ni(Ac)_2{\cdot}4H_2O$ and 78 mg of thiourea were added to 40 mL of ethylenediamine containing 200 mg of the above CdS nanorods. After stirring for 30 min, the achieved suspension was transferred into a 100-mL Teflon-lined stainless steel autoclave, heated at 180 °C and maintained at this temperature for 6 h. After the reaction, the precipitate was obtained by centrifugation and washed with ethanol and DI water several times. Finally, it was dried at 60 °C in the oven and denoted as 1.0 wt% NiS/CdS. The other NiS/CdS samples were synthesized by the same method, except that the amount of $Ni(Ac)_2{\cdot}4H_2O$ was changed. These samples were denoted as 0.1 wt% NiS/CdS, 0.5 wt% NiS/CdS and 3 wt% NiS/CdS, according to the weight ratios of NiS and CdS.

2.3. Characterizations

The thermal programmed desorption (TPD) spectra were obtained with a Quantachrome Instruments Chembet instrument. The concentration of ammonia was detected by Nessler's reagent with a UV-2600 spectrophotometer. The concentration of NO_3^- was detected by dual-wavelength spectrophotometry with a UV-2600 spectrophotometer. The crystal structures of the samples were determined by X-ray diffraction (XRD; Bruker D8 Advance X-ray diffractometer) with Cu Kα radiation ($\lambda = 0.15406$ nm) as the incident beam at 40 kV and 40 mA. The morphologies of the samples were determined by transmission electron microscopy (TEM; FEI Tecnai G2 F30) operated at 150 kV and scanning electron microscopy (SEM; Hitachi FE-SEM SU8000) operated at 10 kV. UV–Vis diffuse reflection spectroscopy (DRS) was carried out with a Shimadzu UV-2600 spectrophotometer using $BaSO_4$ as the reference. The electrochemical measurements were examined with an Autolab PGSTAT302N instrument in a conventional three-electrode cell. It used a carbon electrode as the counter electrode and an Hg/Hg_2Cl_2 electrode as the reference electrode. The electrolyte was 0.5 mol L^{-1} Na_2SO_4. The working electrode was prepared on FTO glass, which had been previously cleaned by sonication in ethanol for 30 min and dried at 100 °C. FTO glass substrates with a coated area of about (1×1) cm^2 were used for both electrodes. Linear sweep voltammograms (LSVs) were obtained from -0.6 to -1.6 V versus Hg/Hg_2Cl_2 (0.5 mol L^{-1} Na_2SO_4) with a scan rate of 10 mV s^{-1}. Electrochemical impedance spectroscopy (EIS) experiments were carried out in the same configuration from 10^5 to 10^{-1} Hz with an AC voltage of 20 mV. Transient photocurrent measurements were carried out in the same configuration. Mott-Schottky values were recorded between -1.0 and 0.5 V versus Hg/Hg_2Cl_2 (0.5 mol L^{-1} Na_2SO_4). The ^{15}N labeling experiments were performed by LC-MS (Agilent 1290 Infinity/6460 LC/QQQ MS). The pH value was determined with a pH meter (PHS-25/3C). The XPS measurements were obtained with a Kratos Axis-Ultra multifunctional X-ray spectrometer.

2.4. Computational methods

All spin unrestricted DFT calculations were performed using the Vienna Ab-initio Simulation Package [32,33] (VASP) with the PBE (Perdew-Burk-Ernzerhof) function [34]. The plane wave basis (the kinetic energy cutoff value was set at 520 eV) and PAW (projector-augmented wave) pseudopotential [35,36] were employed. The atomic positions were fully optimized, except when the Hellmann-Feynman force was <0.05 eV Å^{-1}, and the total energy convergence criteria was set at 1×10^{-4} eV. The two surfaces of CdS (0 0 2) and NiS (2 1 1) were involved in our calculation, and 331 and 221 supercells were used, respectively. The atomic positions of the two top layers were optimized, while the other layers were fixed. To avoid interactions of the neighboring images, an approximate 15-Å vacuum layer was set at the direction of the *c* axis. The Monkhorst-Pack [37] k-point grid $2 \times 2 \times 1$ was set for all calculations.

2.5. Photocatalytic nitrogen fixation reaction

Photocatalytic nitrogen fixation was investigated as previously described [16]. Approximately 100 mg of catalyst (NiS/CdS) was dispersed in 100 mL of pure water under ultrasonication for 15 min. The solution was transferred into a double-walled quartz reactor. Highly pure N_2 was continuously bubbled with a dispersion rate of approximately 100 mL min^{-1}, and then the system was irradiated with a 300 W Xe lamp (Perfect Light Company Solaredge 300C) through the quartz window. The visible light was provided by a Xe lamp with a 420-nm cut-off filter ($\lambda > 420$ nm). All runs were conducted at ambient pressure and 25 °C. A 2-mL portion of liquid was aliquoted from the solution at the indicated times for the measurement of the ammonia level. The concentration of ammonia was detected by the Nessler's reagent method and a UV-2600 spectrophotometer (Shimadzu). The concentration of nitrate was detected by the dual-wavelength spectrophotometry method with a UV-2600 spectrophotometer. The wavelength-dependent nitrogen fixation was also measured in the N_2 fixation system with band-pass filters of 420, 475, 520, 600 and 650 nm. The apparent quantum efficiency (AQE) was estimated using the equation:

$$\text{AQE} = \frac{6 \times \text{the number of evolved ammonia molecules}}{\text{the number of incident photons}} \times 100\%.$$

Cycle tests of the as-prepared composite materials (100 mg) of NiS/CdS were conducted in the nitrogen fixation system. Approximately 100 mg of the NiS/CdS nanoparticles was dispersed into 100 mL of pure water under conditions similar to those of the photocatalytic nitrogen fixation reaction. Approximately 2 mL of liquid was aliquoted from the solution after 1 h of visible light irradiation for the measurement of the ammonia level. The catalyst was collected by centrifugation, and then washed with ethanol and DI water several times. Finally, the recycled catalyst was dried at 60 °C in an oven for 12 h. The recycled catalyst was dissolved in fresh water, and its concentration was maintained constant for the second cycle of the N_2 fixation test. The three cycles of the N_2 fixation test were carried out in the same procedure.

3. Results and discussion

As reported by Zhang et al. [38], vacancies play an important role in photocatalytic N_2 fixation. The CdS nanorods with sulfur vacancies were synthesized in hydrazine solution as previously described. Fig. S1 (online) shows the scanning electron microscopy (SEM) images of the as-prepared CdS nanorods with a length of ~150 nm and a diameter of ~50 nm. Fig. S2 (online) displays the X-ray diffraction (XRD) patterns of the CdS nanorods loaded with different amounts of NiS, which is indexed as the hexagonal wurtzite phase (JCPDS Card No. 41-1049). NiS was loaded onto the surface of CdS by the additional hydrothermal reaction of $Ni(OAc)_2$ and thiourea. There was no apparent change after loading the NiS by another hydrothermal reaction (Fig. S1 online). However, no NiS signal was observed in the XRD patterns, even when ~3.0 wt% NiS was loaded onto CdS. A slight shift toward a large theta (~0.06°) was observed in the XRD patterns, indicating that Ni^{2+} might have entered the lattice of CdS because the ionic radius of Ni^{2+} (72 pm) was smaller than that of Cd^{2+} (95 pm). Energy-dispersive X-ray spectroscopy (EDAX) was carried out. The Ni element observed in the spectra (Fig. S3 online) confirmed the presence of the Ni element in the sample. The diffuse-reflectance (DR) UV–Vis spectra of CdS with different amounts of NiS are shown in Fig. S4 (online). All spectra exhibited broad and strong light absorption in the visible light region, which spanned the UV range to the band edge of ~500 nm. The corresponding optical band gap was 2.37 eV. The band tail gradually increased as the amount of NiS increased.

Fig. 1a–c shows transmission electron microscopy (TEM) and high-resolution (HR) TEM images of NiS/CdS. The low magnification TEM image illustrates the morphology of the CdS nanorods with a length of (136.4 ± 11.4) nm and a diameter of (40.7 ± 4.2) nm. The HR TEM images show the main part with a lattice fringe spacing of 0.335 nm, which was associated with the (0 0 2) of CdS nanorods. A few nanorods with a length of ~10 nm and a width of (1.46 ± 0.2) nm covered the surface of the CdS nanorods. The lattice fringe spacing was 0.22 nm, which was assigned to the (2 1 1) of NiS. At the same time, a few different lattice orientation domains (red circles) were observed on the CdS nanorods. The corresponding lattice fringe spacing was ~0.22 nm. These findings indicated that the morphology of the NiS was in the shape of a nanoflake with a diameter of 5–10 nm and a thickness of ~1.5 nm. Furthermore, X-ray photoelectron spectroscopy (XPS) was employed to verify the composition and valance state. Fig. S5 (online) shows the complete survey of the CdS nanorods before and after loading with NiS nanoflakes. Cd and S signals were observed at 404 and 162 eV, respectively. A weak Ni signal appeared at 857 eV in the NiS/CdS sample. Fig. 1e shows the HR XPS spectra of Cd 3d for the CdS and NiS/CdS nanorods. Two peaks at 404.8 and 411.9 eV corresponded to Cd 3d 5/2 and 3d 3/2, respectively. Each Cd 3d XPS peak could be assigned into two Lorentz peaks, 411.79 and 412.07 eV for Cd 3d3/2 and 404.96 and 404.34 eV for Cd 3d5/2, respectively. Compared with the CdS XPS standard, these binding energy values shifted slightly to lower bonding energies. According to the work of Zhang et al. [38], the components at the lower binding energies (404.34 and 411.79 eV) in the Cd 3d XPS spectra associated with Cd in the low valence or interstitial Cd in the CdS nanorods, indicating that the CdS nanorods contained S vacancies on the surface. Based on these results, we speculated that sulfur vacancies in both CdS and NiS/CdS nanorods existed. A weak Ni signal appeared at 857.6 eV in the HR XPS of Ni 2p in NiS/CdS (Fig. 1f). Based on these characterizations, the NiS nanoflakes were successfully loaded onto the CdS nanorod surface.

According to our hypothesis, NiS nanoflakes function as a cocatalyst within the NiS/CdS composite catalyst. It has three roles in enhancing catalytic activity, namely, enhancing the N_2 absorbance, lowering the reduction potential of N_2 reduction and promoting the charge separation of CdS. Firstly, the adsorption energies of N_2 on the surface of the catalyst were calculated based on the density functional theory (DFT). Fig. 2a shows the theoretical calculation of the N_2 adsorption energy on CdS (0 0 2) and NiS (2 1 1), which was determined by the HR TEM images (Fig. 1d). The results indicate that it is difficult to adsorb N_2 onto the surface of CdS (0 0 2) because its adsorption energy was 1.16 eV (positive), indicating that the N_2 adsorption process on the CdS was not a spontaneous process. However, the adsorption energy on NiS was −0.26 eV, implying that N_2 molecules tend to adsorb onto the NiS surface. The adsorption energy of N_2 molecules on the Ni doped CdS surface was also calculated. The adsorption energy was even lower (−0.55 eV), indicating that N_2 molecules prefer to adsorb onto the Ni doped CdS surface. The temperature programmed desorption (TPD) technique allows one to determine the interaction of gaseous molecules with the solid surface. Therefore, TPD is a powerful tool to evaluate the active sites on the catalyst surface and to understand the reaction mechanism, which involves adsorption,

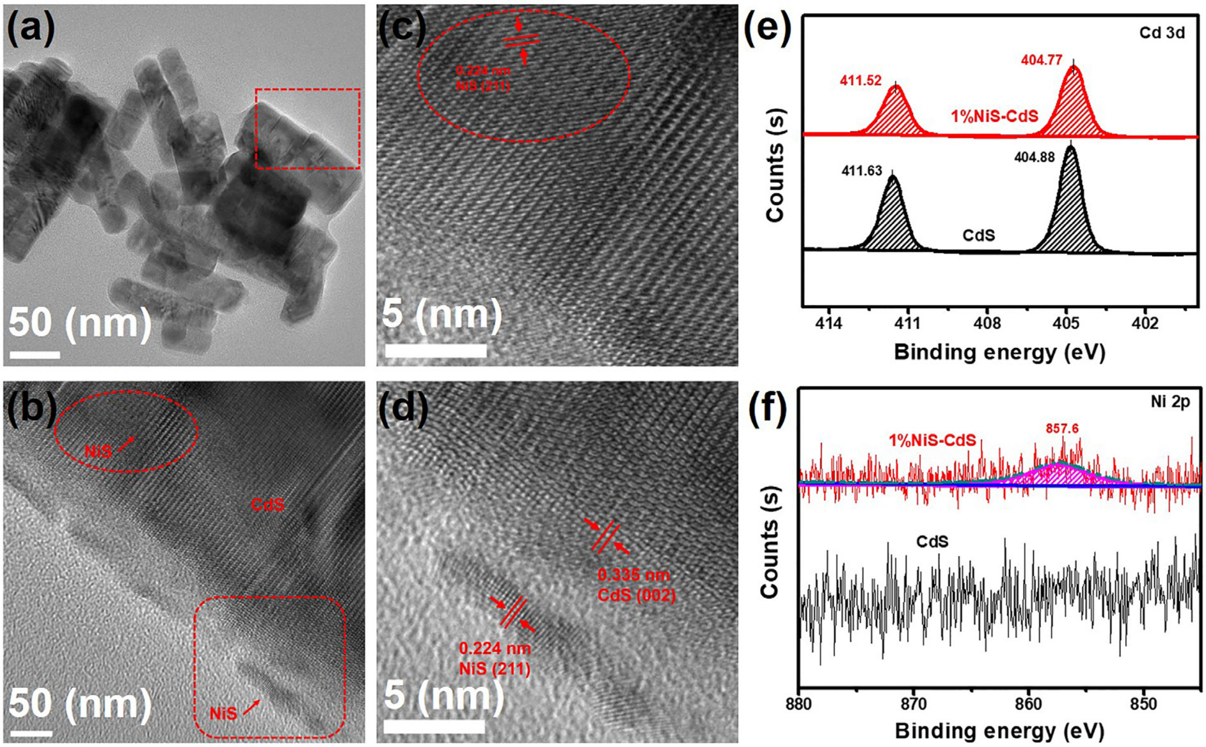

Fig. 1. Characterization of NiS/CdS. Transmission electron microscopy (TEM) and high resolution (HR) TEM images of NiS/CdS (a–d). High resolution X-ray photoelectron spectrum (XPS) of Cd 2p (e) and Ni 2p (f) for CdS and NiS/CdS.

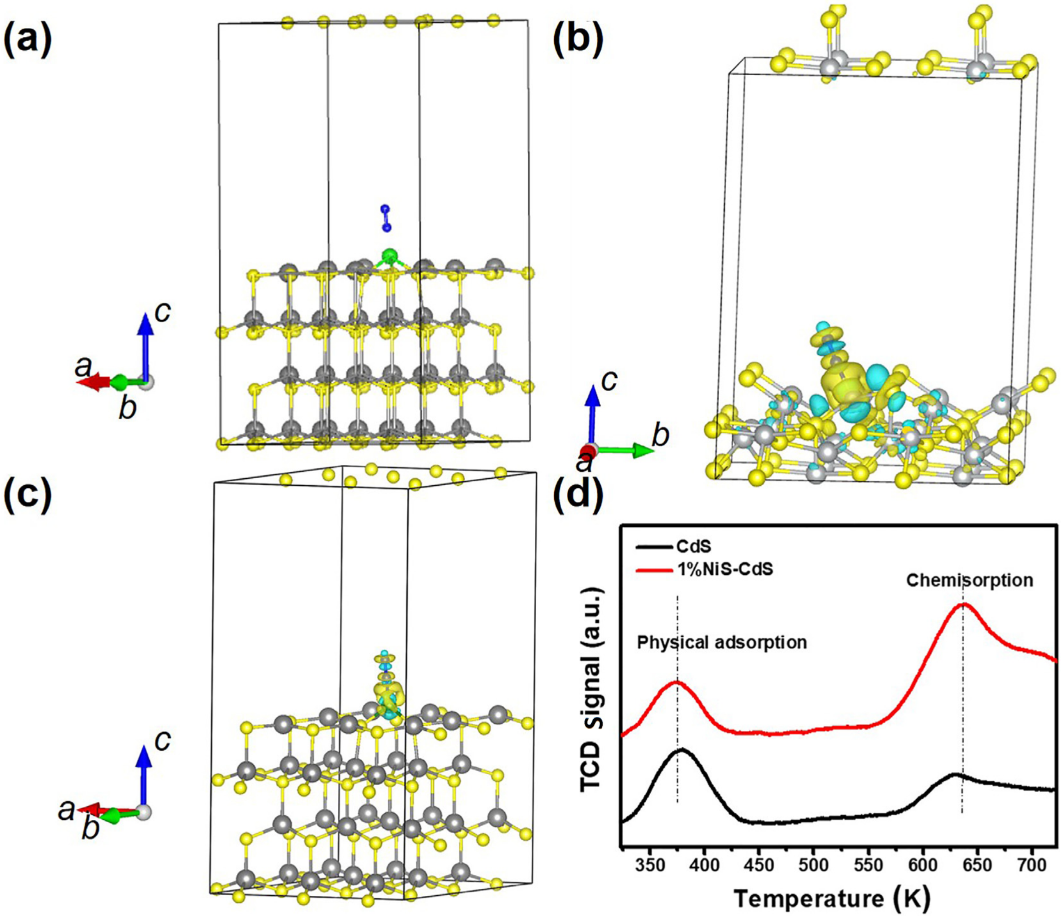

Fig. 2. N_2 adsorption on CdS and NiS/CdS nanorods. The theoretical adsorption energy of N_2 molecules on the CdS (0 0 2) surface (a), NiS (2 1 1) surface (b) and Ni doped CdS (0 0 2) surface (c). (d) Temperature programmed desorption (TPD) curves of N_2 on CdS and NiS/CdS.

surface reaction and desorption. The TPD behavior of N_2 on the CdS nanorod and NiS/CdS is shown in Fig. 2b. Both samples exhibited two desorption peaks of N_2. The desorption peaks at 377 K were related to the physical adsorption. The corresponding peak area was about 12.0 and 11.9, respectively, indicating that the physical adsorption of N_2 on CdS and NiS/CdS was similar. The peaks at 631 and 637 K were assigned to the chemical adsorption of N_2 on CdS and NiS/CdS surfaces, respectively. However, the peak areas were 5.4 and 25.1 for CdS and NiS/CdS, respectively. Although the adsorption energy of the N_2 molecule onto the CdS (0 0 2) surface was a positive value according to the theoretical calculation, the defects on the surface might have resulted in the adsorption of the N_2 molecule. TPD results confirmed that N_2 had a much stronger adsorption on NiS/CdS than that on pure CdS. Both theoretical and experimental results illustrated that N_2 molecules preferred to adsorb onto the NiS/CdS surface.

The electrochemical N_2 reduction reaction (NRR) test was performed to determine the nitrogen reduction ability of the catalyst CdS and NiS/CdS by linear sweep voltammetry (LSV). LSV measurements (Fig. 3a) were carried out in an Ar and N_2 saturated environment to distinguish between HER and NRR. When the potential was <-0.69 and -0.46 V vs. RHE in the Ar saturated environment, the current density increased for both CdS and NiS/CdS, indicating that HER occurs at these potentials. In the case of the N_2 saturated solution, the current density increased to about -0.68 V vs. RHE for CdS, indicating that NRR hardly occurred for CdS due to the competition of HER. In the case of NiS/CdS, NRR could occur at a potential as low as -0.33 V vs. RHE. Compared with CdS, the NRR overpotential decreased significantly by introducing the co-catalyst of NiS. With regard to the NiS/CdS sample, the LSV curves intersected at -0.88 V vs. RHE under an Ar and N_2 saturated environment, indicating that the NRR occurred at a more positive value than that of HER. HER superseded RHE when the potential was more negative than the potential of RHE (-0.88 V vs. RHE) [39,40]. Thus, NRR should be carried out in the potential range from -0.88 to -0.33 V vs. RHE for NiS/CdS. Based on the LSV, NiS dramatically decreased the overpotential for the NRR reaction, which agreed with the theoretical and TPD results because a high N_2 adsorption resulted in high NRR activity.

To determine the function of NiS, transient photocurrent and electrochemical impedance spectroscopy (EIS) were used. CdS and NiS/CdS were deposited onto the FTO for the photoelectrode. As shown in Fig. 3b, the CdS sample displayed a weak photocurrent response due to the rapid recombination of the photogenerated charge carrier. NiS/CdS provided a much higher photocurrent density than CdS, which confirmed the enhanced separation and transfer of the photogenerated electron and holes in the NiS/CdS sample. These findings indicate that the NiS co-catalyst effectively promoted the charge separation for the composite photocatalyst NiS/CdS [30]. This was beneficial to photocatalysis, thereby enhancing the efficiency of photocatalytic NRR. The role of NiS in prompting charge separation and transfer can also be reflected by the EIS spectra. The EIS Nyquist plots of CdS and NiS/CdS are presented in Fig. 2c. As shown in the equivalent circuit (inset, Fig. 3c), the charge transfer resistance (R_p) at the catalyst/electrolyte interface could be evaluated by the semicircle radius of the Nyquist plots based on the R-C equivalent circuit. The corresponding R_p values are listed in Table S1 (online). The R_p of CdS was 980 Ω, which was related to the characteristics of CdS. After loading NiS, the R_p decreased to 782 Ω, which revealed a lower resistance. These findings indicated that NiS/CdS had a better charge separation efficiency than pure CdS. Furthermore, the R_p decreased to 624 Ω after exposure to light irradiation, implying that light can further promote the charge separation process. Based on these results, NiS can enhance N_2 adsorption, lower the overpotential of the N_2 reduction reaction and promote the charge separation process. Thus, NiS functions as a co-catalyst in the photocatalytic N_2 reduction reaction.

The next issue was assessing the photocatalytic activity of NiS/CdS for N_2 fixation because NiS could function as a co-catalyst in photocatalysis. Photocatalytic experiments were performed in N_2 saturated water under full-spectrum and visible light ($\lambda > 420$ nm) irradiation at ambient conditions without any sacrificial agent. The ammonia concentration was measured by the Nessler's reagent method, and the calibration curves are shown in Fig. S6 (online). Fig. 4a shows the photocatalytic N_2 fixation of CdS in the presence of different amounts of NiS. CdS exhibited a weak photocatalytic activity of 0.03 mg L^{-1} within the first hour. After loading 1.0 wt% NiS, the photocatalytic activity increased significantly to 2.8 mg L^{-1} within the first hour of irradiation. However, the ammonia production rate decreased with the increase of the reaction time. To understand the reason for the decrease in the ammonia production rate, the pH of the solution was monitored with the reaction time. The pH continued to increase from 6.7 to 7.8 over 12 h of the photocatalytic reaction due to the production of ammonia (Fig. S7 online). According to the results of Hirakawa et al. [15] a high pH can depress the photocatalytic NRR reaction. Thus, the increasing pH resulted in a decrease of the N_2 fixation rate in the reaction solution. Accompanied by the NRR reaction of the photogenerated electron, an oxidation reaction involving the holes might have occurred to balance the charge, which would include water oxidation and ammonia oxidation. To confirm the ammonia oxidation reaction, NO_3^- was detected by the spectral method according to GB11894-89, China M. HJ, 2012, 636: 2012. The calibration curve of NO_3^- is shown in Fig. S8 (online). Fig. S9 exhibits the NO_3^- concentration increase with the reaction time for NiS/CdS. No NO_3^- was detected for CdS as a photocatalyst. These findings indicate that ammonia was oxidized by the photogenerated holes when the ammonia concentration reached a certain value. Thus, we conjecture that an increased

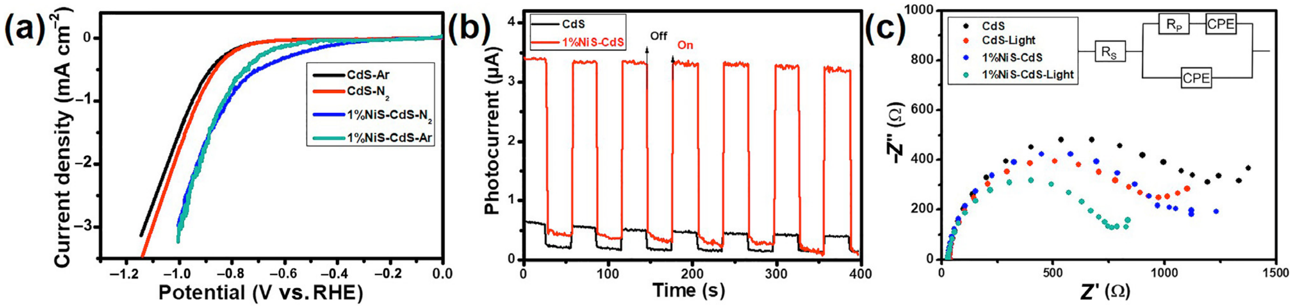

Fig. 3. Electrochemical performance of the photocatalysts. (a) Linear sweep voltammetry of CdS and NiS under an Ar and N_2 saturated solution. (b) Transient photocurrent of CdS and NiS/CdS. (c) Electrochemical impedance spectroscopy of CdS and NiS/CdS under light irradiation and dark conditions.

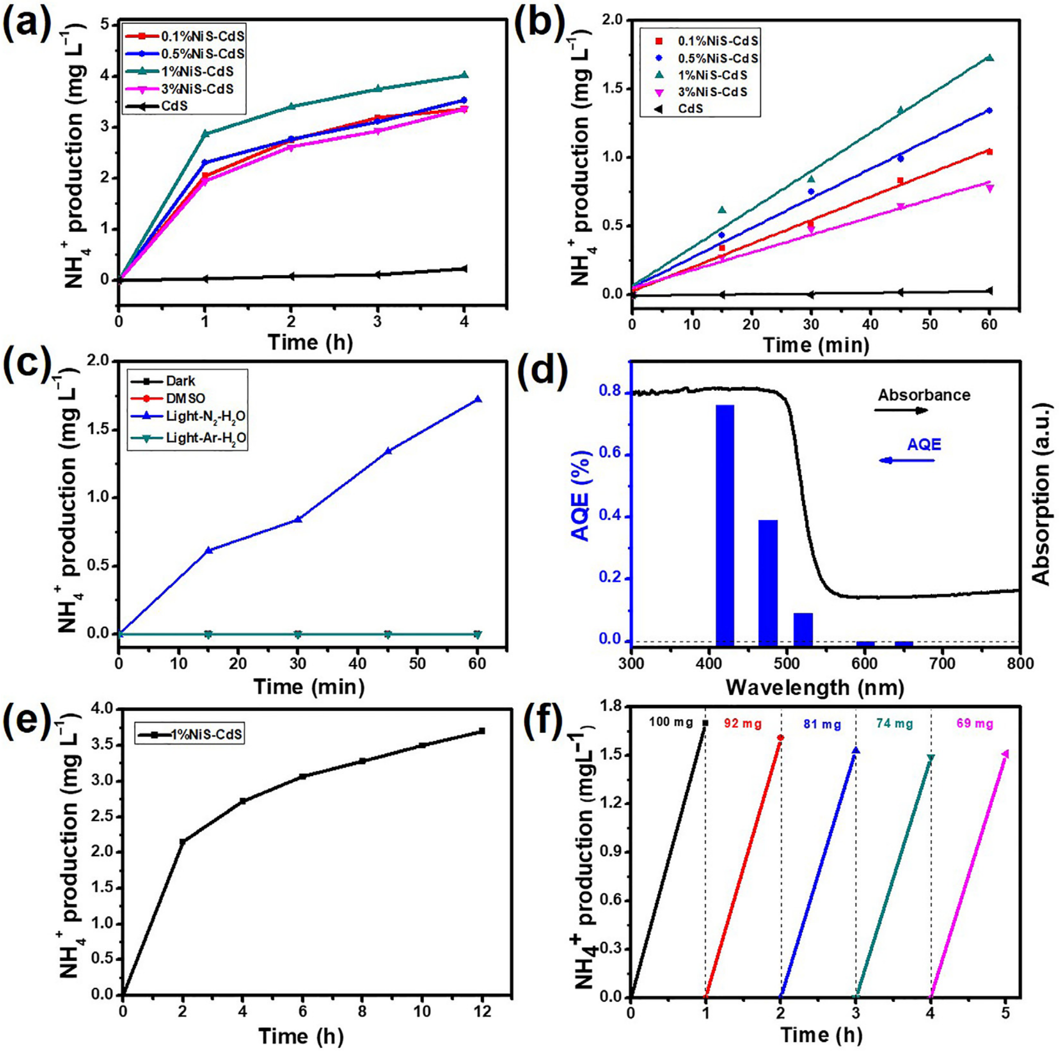

Fig. 4. Photocatalytic performance of the photocatalysts. (a) NH_4^+ production changes with the reaction time under full spectrum light irradiation. (b) NH_4^+ production changes with the reaction time under the visible light irradiation ($\lambda > 420$ nm) within 1 h. (c) NH_4^+ production under different conditions (darkness, DMSO as solvent and water + light + N_2 or Ar) and exposure to visible light. (d) Apparent quantum efficiency (AQE) of NiS/CdS under visible light with different band pass filters (420, 475, 520, 600 and 650 nm). (e) NH_4^+ production changes with the reaction time under visible light irradiation ($\lambda > 420$ nm) for 12 h. (f) Recycling experiment of NiS/CdS for five continuous cycles under visible light irradiation. The catalyst amounts were 100, 92, 81, 74 and 69 mg, respectively. The reaction dispersion concentration was maintained at 1 mg mL^{-1} for the five cycles.

pH and ammonia oxidation were the main reasons for the decrease in the ammonia production rate with the increase of reaction time. Thus, CdS was recognized as a visible light photocatalyst with a light adsorption range that can reach 550 nm. The visible light photocatalytic N_2 fixation process is shown in Fig. 4b. Pure CdS exhibited almost zero N_2 fixation in the visible light irradiation range ($\lambda > 420$ nm) within 1 h. After loading NiS, N_2 fixation activity was enhanced significantly. The N_2 fixation rate reached ~1.0 mg L^{-1} h^{-1} after loading 0.1 wt% NiS. It further increased to ~1.7 mg L^{-1} h^{-1} after loading 1.0 wt% NiS. However, an excessive amount of NiS resulted in a decreased N_2 fixation rate.

To confirm the light and water functions, the photocatalytic N_2 fixation reaction was performed in the dark and in the presence of DMSO solution, respectively. As shown in Fig. 4c, no ammonia was detected both in the dark and the DMSO-containing solution, indicating that no ammonia was produced without light irradiation and water. According to the mechanism of N_2 fixation [5,13]. CdS was excited by light to produce the excited electron for the reduction of N_2 and water to provide the proton to produce the ammonia. Thus, light and water are required for the N_2 fixation reaction. The apparent quantum efficiency (AQE) was measured at different wavelengths in the visible region. The AQEs were 0.76%, 0.39% and 0.09% at 420, 475 and 520 nm, respectively, which agree with the UV–Vis absorption spectrum of NiS/CdS. For the stability of catalyst is characterization as well. Fig. 3e shows that the amount of ammonia increased after 12 h of exposure to visible light irradiation ($\lambda > 420$ nm). It also exhibits a gradual decrease in the N_2 fixation rate with a continuous increase of the reaction time because the pH continued to increase and the as-produced ammonia could be oxidized in the reaction solution. To characterize the stability of the catalyst, another method was employed. Each cycle was carried out for 1 h and then the catalyst was recycled by centrifugation, washed with water and ethanol and dried at 60 °C for >12 h. The recycled catalyst was dissolved in fresh water, and its concentration was maintained constant for the second cycle of the N_2 fixation test. Fig. 3f shows the results of the NiS/CdS cyclic experiment after five cycles of visible light irradiation ($\lambda > 420$ nm). The catalyst amount is marked on the graph. Apparently, the degree of N_2 fixation decreased slightly with each cycle. However, it increased when the decrease of the catalyst amount

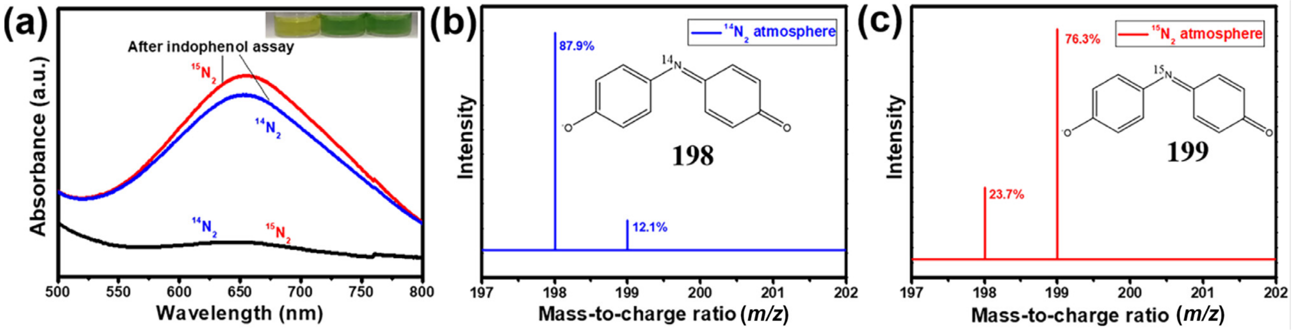

Fig. 5. The mass spectra of the indophenol prepared and UV–Vis absorption spectra from different atmosphere. (a) UV–Vis absorption spectra of the solutions from the nitrogen fixation reaction with $^{14}N_2$ or $^{15}N_2$ gas followed by the indophenol assay. Photos show the color change of the $^{14}N_2$ and $^{15}N_2$ solutions by the indophenol assay. MS spectra of derived indophenol solutions from (b) $^{14}N_2$ and (c) $^{15}N_2$.

was taken into account. In the first cycle, the ammonia concentration was about 1.7 mg L^{-1} for 100 mg of catalyst within 1 h. After five cycles, the ammonia concentration was about 1.5 mg L^{-1} for 69 mg of catalyst within 1 h. Thus, there was no obvious decrease in activity as evidenced by the five continuous photocatalytic cycles [19].

To confirm the origin of the ammonia from N_2 in the current system, a photocatalytic N_2 fixation reaction was carried out with isotope-labeled $^{15}N_2$ gas as previously described [15,41,42]. Approximately 30 mg of catalyst was dispersed in 30 mL of water by ultrasonication for 15 min. The reaction solution was transferred into a reactor and bubbled with Ar for 30 min. The closed system reactor was turned on. Thereafter, 30 mL of $^{15}N_2$ gas was injected into the closed reactor and light irradiated for 55 h. The control sample was obtained by injecting 30 mL of high pure N_2 gas. The as-prepared ammonia amounts were 6.8 and 6.7 mg L^{-1} for $^{15}N_2$ and $^{14}N_2$, respectively, indicating that the amounts of ammonia from both N_2 sources were similar. The obtained solution (0.5 mL) reacted with 0.1 mL of a 1.0% phenolic solution in the presence of NaClO as the oxidant and $Na(Fe(CN)_5NO)$ as the catalyst. As shown in Fig. 4a, both solutions showed a clear absorption peak at 660 nm that corresponded to indophenol. However, no adsorption peak was observed for both solutions in the absence of light irradiation. The respective solutions were characterized by liquid chromatography-mass spectroscopy (LC-MS). Fig. 5b and c display the MS spectra of the indophenol solution from $^{14}N_2$ and $^{15}N_2$. The $^{14}N_2$ solution exhibited two peaks at m/z 198 and m/z 199, which were assigned to the indophenol anion. The ratio of ^{14}N:^{15}N was about 88/12 for the $^{14}N_2$ gas, whereas the ratio of ^{14}N:^{15}N was 24/76 for the $^{15}N_2$ gas. These results confirm that the N_2 gas is the source of the ammonia.

4. Conclusions

In this report, we proposed to load co-catalyst NiS nanoflakes on CdS nanorods with defects. The NiS co-catalyst clearly manifested multiple functions in photocatalytic N_2 fixation. The NiS enhanced the adsorption of N_2 molecules on the catalyst surface, and its surface adsorption energy changed from 1.16 to −0.55 eV. The TPD experiment also showed that NiS/CdS possessed a higher chemisorption of N_2. The LSV results indicated that NiS could significantly decrease the overpotential of NRR from −0.88 V to −0.33 V vs. RHE, which effectively promoted NRR. The transient photocurrent and EIS studies showed that NiS could promote the charge separation process of the photocatalytic reaction. Based on the aforementioned results, the photocatalytic N_2 fixation was characterized. The results indicated that NiS/CdS exhibited an excellent N_2 fixation capability, reaching 2.8 and 1.7 mg L^{-1} within the first hour under full spectrum and visible light ($\lambda > 420$ nm) irradiation. Finally, the $^{15}N_2$ isotope labeling experiment revealed that the ammonia originated from N_2.

Conflict of interest

The authors declare that they have no conflict of interest.

Acknowledgments

This work was financially supported by the Beijing Municipal High-Level Innovative Team Building Program (IDHT20180504), the National Natural Science Foundation of China (21805004, 21671011, 21872001 and 51801006), the Beijing Natural Science Foundation (KZ201710005002 and 2192005), the China Postdoctoral Science Foundation (2018M641133), the Beijing Postdoctoral Research Foundation (2018-ZZ-021) and the Chaoyang District Postdoctoral Research Foundation, China (2018-ZZ-026). The Large-Scale Instrument and Equipment Department at the Beijing University of Technology was also acknowledged.

Author contributions

X. Gao, D. Qu and Z. Sun conceived and designed the photocatalytic N_2 fixation experiments. X. Gao performed the most experiments. Y. Chai, L. An and S. Sun carried theoretical calculation. W. Jiang and Y. Wen assisted with the material characterizations and data analysis. S. Sun and X. Liu gave the constructive comments on the manuscript. All authors contributed to the discussion.

Appendix A. Supplementary data

Additional characterizations by SEM, XRD, EDAX, UV-Vis spectra and XPS, as well as the calibration curve as PDFs, can be found online at https://doi.org/10.1016/j.scib.2019.05.009.

References

[1] Pool JA, Lobkovsky E, Chirik PJ. Hydrogenation and cleavage of dinitrogen to ammonia with a zirconium complex. Nature 2004;427:527.
[2] Honkala K, Hellman A, Remediakis IN, et al. Ammonia synthesis from first-principles calculations. Science 2005;307:555–8.
[3] Schrauzer GN, Guth TD. Photolysis of water and photoreduction of nitrogen on titanium dioxide. J Am Chem Soc 1977;99:7189.
[4] Bickley RI, Vishwanathan V. Photocatalytically induced fixation of molecular nitrogen by near uv radiation. Nature 1979;280:306–8.
[5] Wang S, Ichihara F, Pang H, et al. Nitrogen fixation reaction derived from nanostructured catalytic materials. Adv Funct Mater 2018;28:1803309.
[6] Li H, Li J, Ai Z, et al. Oxygen vacancy-mediated photocatalysis of biocl: reactivity, selectivity, and perspectives. Angew Chem Int Ed 2018;57:122–38.

[7] Liu J, Kelley MS, Wu W, et al. Nitrogenase-mimic iron-containing chalcogels for photochemical reduction of dinitrogen to ammonia. Proc Natl Acad Sci USA 2016;113:5530–5.

[8] Zhang N, Jalil A, Wu D, et al. Refining defect states in $W_{18}O_{49}$ by Mo doping: a strategy for tuning N_2 activation towards solar-driven nitrogen fixation. J Am Chem Soc 2018;140:9434–43.

[9] Zhu D, Zhang L, Ruther RE, et al. Photo-illuminated diamond as a solid-state source of solvated electrons in water for nitrogen reduction. Nat Mater 2013;12:836–41.

[10] Li H, Shang J, Ai Z, et al. Efficient visible light nitrogen fixation with biobr nanosheets of oxygen vacancies on the exposed 001 facets. J Am Chem Soc 2015;137:6393–9.

[11] Medford AJ, Hatzell MC. Photon-driven nitrogen fixation: current progress, thermodynamic considerations, and future outlook. ACS Catal 2017;7:2624–43.

[12] Li H, Shang J, Shi J, et al. Facet-dependent solar ammonia synthesis of biocl nanosheets via a proton-assisted electron transfer pathway. Nanoscale 2016;8:1986–93.

[13] Li J, Li H, Zhan G, et al. Solar water splitting and nitrogen fixation with layered bismuth oxyhalides. Acc Chem Res 2017;50:112–21.

[14] Sun S, An Q, Wang W, et al. Efficient photocatalytic reduction of dinitrogen to ammonia on bismuth monoxide quantum dots. J Mater Chem A 2017;5:201–9.

[15] Hirakawa H, Hashimoto M, Shiraishi Y, et al. Photocatalytic conversion of nitrogen to ammonia with water on surface oxygen vacancies of titanium dioxide. J Am Chem Soc 2017;139:10929–36.

[16] Gao X, Wen Y, Qu D, et al. Interference effect of alcohol on nessler's reagent in photocatalytic nitrogen fixation. ACS Sustain Chem Eng 2018;6:5342–8.

[17] Li X, Wang W, Jiang D, et al. Efficient solar-driven nitrogen fixation over carbon–tungstic-acid hybrids. Chem Eur J 2016;22:13819–22.

[18] Ling C, Niu X, Li Q, et al. Metal-free single atom catalyst for N_2 fixation driven by visible light. J Am Chem Soc 2018;140:14161–8.

[19] Zhao Y, Zhao Y, Waterhouse GIN, et al. Layered-double-hydroxide nanosheets as efficient visible-light-driven photocatalysts for dinitrogen fixation. Adv Mater 2017;29:1703828.

[20] Lu Y, Yang Y, Zhang T, et al. Photoprompted hot electrons from bulk cross-linked graphene materials and their efficient catalysis for atmospheric ammonia synthesis. ACS Nano 2016;10:10507–15.

[21] Oshikiri T, Ueno K, Misawa H. Selective dinitrogen conversion to ammonia using water and visible light through plasmon-induced charge separation. Angew Chem Int Ed 2016;55:3942–6.

[22] Martirez JMP, Carter EA. Prediction of a low-temperature N_2 dissociation catalyst exploiting near-ir–to–visible light nanoplasmonics. Sci Adv 2017;3:eaao4710.

[23] Chen X, Shen S, Guo L, et al. Semiconductor-based photocatalytic hydrogen generation. Chem Rev 2010;110:6503–70.

[24] Tong H, Ouyang S, Bi Y, et al. Nano-photocatalytic materials: possibilities and challenges. Adv Mater 2012;24:229–51.

[25] Kou J, Lu C, Wang J, et al. Selectivity enhancement in heterogeneous photocatalytic transformations. Chem Rev 2017;117:1445–514.

[26] Zhang P, Wang T, Chang X, et al. Effective charge carrier utilization in photocatalytic conversions. Acc Chem Res 2016;49:911–21.

[27] Wang J, Xia T, Wang L, et al. Enabling visible-light-driven selective CO_2 reduction by doping quantum dots: trapping electrons and suppressing H_2 evolution. Angew Chem Int Edit 2018;57:16447–51.

[28] Yang J, Wang D, Han H, et al. Roles of cocatalysts in photocatalysis and photoelectrocatalysis. Acc Chem Res 2013;46:1900–9.

[29] Ding C, Shi J, Wang Z, et al. Photoelectrocatalytic water splitting: significance of cocatalysts, electrolyte, and interfaces. ACS Catal 2016;7:675–88.

[30] Liu M, Chen Y, Su J, et al. Photocatalytic hydrogen production using twinned nanocrystals and an unanchored NiS_x co-catalyst. Nat Energy 2016;1:16151.

[31] Maeda K, Domen K. Development of novel photocatalyst and cocatalyst materials for water splitting under visible light. Bull Chem Soc Jpn 2016;89:627–48.

[32] Kresse G, Hafner J. Ab initio molecular dynamics for liquid metals. Phys Rev B 1993;47:558–61.

[33] Kresse G, Furthmüller J. Efficiency of ab-initio total energy calculations for metals and semiconductors using a plane-wave basis set. Comput Mater Sci 1996;6:15–50.

[34] Perdew JP, Burke K, Ernzerhof M. Generalized gradient approximation made simple. Phys Rev Lett 1996;77:3865–8.

[35] Kresse G, Joubert D. From ultrasoft pseudopotentials to the projector augmented-wave method. Phys Rev B 1999;59:1758–75.

[36] Blöchl PE. Projector augmented-wave method. Phys Rev B 1994;50:17953–79.

[37] Monkhorst HJ, Pack JD. Special points for brillouin-zone integrations. Phys Rev B 1976;13:5188–92.

[38] Zhang X, Zhao Z, Zhang W, et al. Surface defects enhanced visible light photocatalytic h2production for Zn-Cd-S solid solution. Small 2016;12:793–801.

[39] Nazemi M, Panikkanvalappil SR, El-Sayed MA. Enhancing the rate of electrochemical nitrogen reduction reaction for ammonia synthesis under ambient conditions using hollow gold nanocages. Nano Energy 2018;49:316–23.

[40] Han J, Liu Z, Ma Y, et al. Ambient N_2 fixation to NH_3 at ambient conditions: using Nb_2O_5 nanofiber as a high-performance electrocatalyst. Nano Energy 2018;52:264–70.

[41] Zhao Y, Shi R, Bian X, et al. Ammonia detection methods in photocatalytic and electrocatalytic experiments: How to improve the reliability of NH_3 production rates? Adv Sci 2019;6:1802109.

[42] Zhao Y, Zhao Y, Shi R, et al. Tuning oxygen vacancies in ultrathin TiO_2 nanosheets to boost photocatalytic nitrogen fixation up to 700 nm. Adv Mater 2019;31:1806482.

Xiang Gao received his B.S. degree in polymer material and engineering from College of Chemistry, Jilin University in 2013. He is studying for his doctorate in condensed matter physics in Changchun Institute of Optics, Fine Mechanics and Physics, Chinese Academy of Sciences under the supervision of Prof. Zaicheng Sun and Xingyuan Liu. His current research interest is CdS based photocatalysts.

Dan Qu received her B.S. degree in polymer material and engineering from College of Chemistry, Jilin University in 2012 and Ph.D. degree in condensed matter physics from Changchun Institute of Optics, Fine Mechanics and Physics, Chinese Academy of Sciences in 2017 under the supervision of Prof. Zaicheng Sun. Currently, she is working at Beijing University of Technology. Her research interests include the controlled synthesis of fluorescent carbon dots and their applications.